ARTICLE

Synthesis of poly(stearyl methacrylate)-poly(2-hydroxypropyl methacrylate) diblock copolymer nanoparticles via RAFT dispersion polymerization of 2-hydroxypropyl methacrylate in mineral oil

Received 00th January 20xx,
Accepted 00th January 20xx

DOI: 10.1039/x0xx00000x

Csilla György, Saul J. Hunter, Chloé Girou, Matthew J. Derry and Steven P. Armes*

Poly(stearyl methacrylate)-poly(2-hydroxypropyl methacrylate) (PSMA-PHPMA) diblock copolymer nanoparticles are synthesized *via* reversible addition-fragmentation chain transfer (RAFT) dispersion polymerization of 2-hydroxypropyl methacrylate (HPMA) in mineral oil at 90 °C. The relatively short PSMA precursor (mean degree of polymerization = 9) remains soluble in mineral oil, whereas the growing PHPMA block quickly becomes insoluble, resulting in polymerization induced self-assembly (PISA). Relatively high HPMA monomer conversions (≥ 98%) were achieved within 70 min as confirmed by *in situ* ^{1}H NMR spectroscopy studies, while gel permeation chromatography (GPC) analyses indicated high blocking efficiencies and relatively narrow molecular weight distributions ($M_w/M_n \leq 1.37$) for all PISA syntheses. Depending on the precise synthesis conditions, this PISA formulation can produce diblock copolymer spheres, worms or vesicles; a pseudo-phase diagram has been constructed to enable reproducible targeting of each pure phase. Thus this is the first example of the use of a commercially available polar monomer for PISA syntheses in non-polar media that offers access to the full range of copolymer morphologies. The resulting nanoparticles were characterized using dynamic light scattering (DLS), transmission electron microscopy (TEM), oscillatory rheology and small-angle X-ray scattering (SAXS). Interestingly, PSMA-PHPMA worms undergo an unusual (partial) worm-to-vesicle transition at elevated temperature. Finally, $PSMA_9$-$PHPMA_{50}$ spheres were evaluated as putative Pickering emulsifiers. Using lower water volume fractions produced water-in-oil (w/o) emulsions after high shear homogenization, as expected. However, using higher water volume fractions, shear rates or copolymer concentrations favored the formation of w/o/w Pickering double emulsions.

Introduction

It is well-known that AB diblock copolymers undergo self-assembly in a selective solvent.[1,2] This provides access to a range of diblock copolymer morphologies, with spheres, worms and vesicles being the most common.[3–5] The preferred copolymer morphology is usually dictated by the relative volume fractions of the two blocks, as indicated by the geometric packing parameter.[6] However, such diblock copolymer nano-objects are typically generated in highly dilute solution (< 1%) using various post-polymerization processing techniques, such as a solvent switch,[4] a pH switch[7] or thin film rehydration.[8] This is a significant problem that has hitherto hindered industrial scale-up for potential applications.

Dainton Building, Department of Chemistry, The University of Sheffield, Brook Hill, Sheffield, South Yorkshire, S3 7HF, UK. E-mail: s.p.armes@shef.ac.uk

Electronic Supplementary Information (ESI) available: PSMA polymerization kinetics; semi-logarithmic plots for RAFT dispersion polymerization of HPMA and BzMA; summary tables of copolymer characterization; further TEM evidence for the partial worm-to-vesicle transition of $PSMA_9$–$PHPMA_{70}$ worms obtained after oscillatory rheology studies; digital photographs of the visual appearance of the Pickering emulsions; further fluorescence microscopy evidence for a w/o/w Pickering double emulsion; droplet diameter *vs*. copolymer concentration plot for w/o Pickering emulsions. See DOI: 10.1039/x0xx00000x

In principle, polymerization-induced self-assembly (PISA)[9–12] offers a highly convenient route to diblock copolymer nano-objects at up to 50% w/w solids. PISA utilizes controlled living radical polymerization techniques such as reversible addition-fragmentation chain transfer (RAFT) polymerization.[13–15] Selecting a suitable solvent for the respective monomer building blocks is critical for a successful PISA formulation: the precursor 'A' block requires a good solvent to act as an effective steric stabilizer while the growing 'B' block requires a non-solvent. Initially, the diblock copolymer chains are fully soluble, because unreacted monomer acts as a co-solvent. However, a critical degree of polymerization is eventually attained whereby the 'B' block becomes insoluble, driving *in situ* self-assembly to produce a colloidal dispersion of sterically-stabilized nanoparticles.

The design rules for PISA are generic: such syntheses can be in a wide range of solvents, including water, lower alcohols and mixtures thereof.[11,16–21] Recently, we have studied RAFT dispersion polymerization in various non-polar media such as *n*-alkanes,[22–26] poly(α-olefins),[12] mineral oil[12,27–30] or low-viscosity silicone oil.[31] Potential applications include next-generation nanoparticle lubricants for automotive engine oils,[30] a new high-temperature oil-thickening mechanism[27] and novel viscosity modifiers for silicone oils.[31]

Poly(2-hydroxypropyl methacrylate) (PHPMA) has been utilized for a wide range of PISA formulations.[32–42] For example, Blanazs *et al.* studied the evolution of copolymer morphology during the RAFT aqueous dispersion polymerization of HPMA, which provided important mechanistic insights regarding the worm-to-vesicle transition.[32] In closely-related work, using PHPMA as a weakly hydrophobic structure-directing block enables the rational design of thermoresponsive worms[33,35,36] and vesicles.[34] Moreover, utilizing PHPMA in conjunction with highly biocompatible steric stabilizer blocks such as poly(glycerol monomethacrylate) [PGMA][43] or poly(ethylene glycol) [PEG][37,44] enable the soft hydrogels formed by semi-concentrated worm dispersions[45] to be evaluated as novel cell storage media.[44,46–48] Zehm and co-workers demonstrated that PHPMA can also be used as a steric stabilizer block for the RAFT alcoholic dispersion polymerization of benzyl methacrylate.[42] Rymaruk *et al.* briefly reported that PHPMA could serve as a core-forming block when exploring RAFT dispersion polymerization formulations in silicone oil.[31] However, only kinetically-trapped spheres could be obtained in this latter case. As far as we are aware, the current study is the first to report the use of PHPMA as a structure-directing block to access spheres, worms or vesicles *via* RAFT-mediated PISA in non-polar media.

Pickering emulsions are particle-stabilized emulsions and have been recognized for more than a century.[49,50] It is well-known that the type of emulsion obtained depends on the particle contact angle, which is in turn dictated by the nanoparticle wettability.[51] Since 2012, various types of diblock copolymer nano-objects have been evaluated as Pickering emulsifiers.[52–55] For example, hydrophilic diblock copolymer nanoparticles prepared *via* aqueous PISA enable the formation of oil-in-water (o/w) Pickering emulsions.[53–55] In contrast, hydrophobic nanoparticles prepared in non-polar solvents such as *n*-alkanes or mineral oil favour the formation of water-in-oil (w/o) emulsions.[56,57] Interestingly, Thompson *et al.* utilized hydrophobic and hydrophilic worms in turn to prepare water-in-oil-in-water (w/o/w) Pickering emulsions.[58]

Herein, we report the synthesis of $PSMA_9$-$PHPMA_x$ diblock copolymer nano-objects *via* RAFT dispersion polymerization of HPMA in mineral oil at 90 °C. Using a relatively short $PSMA_9$ precursor block ensures access to spheres, worms and vesicles.[28] A pseudo-phase diagram has been constructed for a series of $PSMA_9$-$PHPMA_x$ nanoparticles by varying the copolymer concentration from 15% to 30% w/w, confirming that a pure worm phase can be obtained over a relatively narrow range of diblock copolymer compositions (x = 67 to 70). The thermoresponsive nature of such worms is briefly explored and $PSMA_9$-$PHPMA_{50}$ spheres are evaluated as putative Pickering emulsifiers.

Experimental

Materials

2-Hydroxypropyl methacrylate (HPMA) was donated by GEO Specialty Chemicals (UK) and used without further purification. Stearyl methacrylate (SMA) was purchased from Santa Cruz Biotechnology Ltd (USA). Benzyl methacrylate (BzMA, 96%) was purchased from Sigma Aldrich, passed through an inhibitor remover column to remove monomethyl ether hydroquinone (MMEHQ) and then stored at −20 °C prior to use. 2-Cyano-2-propyl dithiobenzoate (CPDB), $CDCl_3$ and *n*-dodecane were purchased from Sigma Aldrich (UK). 2,2'-Azoisobutyronitrile (AIBN) was obtained from Molekula (UK). *tert*-Butyl peroxy-2-ethylhexanoate (T21s) was purchased from AkzoNobel (The Netherlands). CD_2Cl_2 was purchased from Goss Scientific (UK). API Group III mineral oil (viscosity = 3.1 cSt at 100 °C) was kindly provided by The Lubrizol Corporation Ltd (Hazelwood, Derbyshire, UK). All other solvents were purchased from Fisher Scientific (UK) and were used as received.

Synthesis of poly(stearyl methacrylate) ($PSMA_9$) precursor *via* RAFT solution polymerization

The synthesis of the $PSMA_9$ homopolymer precursor was conducted at 50% w/w solids as follows. SMA (34.0 g; 100.4 mmol), CPDB (4.40 g; 19.9 mmol; target degree of polymerization = 5), AIBN (659 mg; 4.01 mmol; CPDB/AIBN molar ratio = 5.0) and toluene (39 g) were weighed into a 250 mL round-bottomed flask. The sealed reaction vessel was purged with nitrogen for 30 min, then placed in a pre-heated oil-bath at 70 °C and stirring for 4 h. The SMA polymerization was quenched by exposing the reaction solution to air and cooling to room temperature. A final SMA conversion of 77% was determined by ^{1}H NMR spectroscopy. The crude homopolymer was purified by two consecutive precipitations into a ten-fold excess of ethanol. The mean degree of

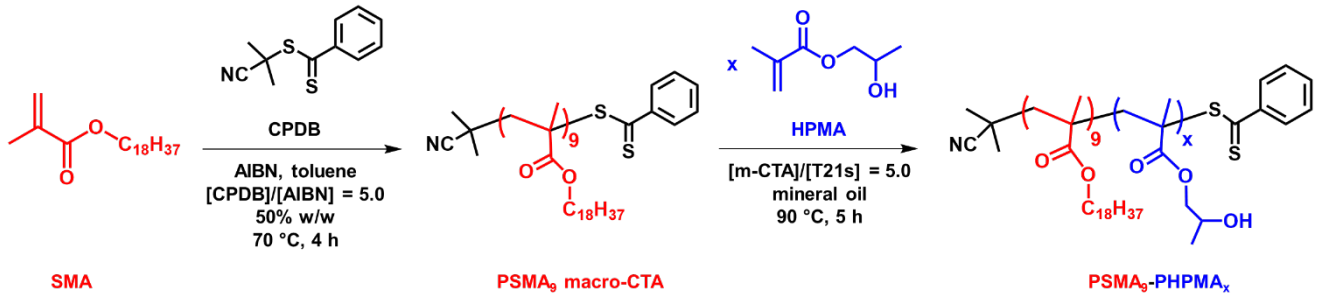

Scheme 1. Synthesis of a poly(stearyl methacrylate) (PSMA) precursor *via* RAFT solution polymerization in toluene using 2-cyano-2-propyl benzodithioate (CPDB) at 70 °C, followed by the RAFT dispersion polymerization of 2-hydroxypropyl methacrylate (HPMA) in mineral oil at 90 °C.

polymerization (DP) of the macro-CTA was calculated to be 9 using ^{1}H NMR spectroscopy by comparing the integrated aromatic protons from the dithiobenzoate end-group at 6.8-8.0 ppm to the two oxymethylene protons assigned to the SMA residues at 3.6-4.0 ppm. THF GPC analysis using a refractive index detector and a series of near-monodisperse poly(methyl methacrylate) standards indicated an M_n of 4 500 g mol^{-1} and an M_w/M_n of 1.12.

Synthesis of poly(stearyl methacrylate)-poly(2-hydroxypropyl methacrylate) ($PSMA_9$-$PHPMA_x$) diblock copolymer nanoparticles *via* RAFT dispersion polymerization of HPMA in mineral oil

The protocol for the synthesis of $PSMA_9$-$PHPMA_{150}$ diblock copolymer vesicles at 15% w/w solids is representative and was conducted as follows. $PSMA_9$ (0.040 g; 12.2 µmol), HPMA (0.26 g; 1.84 mmol), T21s initiator (0.53 mg; 2.45 µmol; 10.0% v/v in mineral oil) and mineral oil (1.73 g) were weighed into a vial and this reaction mixture was purged with nitrogen gas for 30 min. The sample vial was then immersed into a pre-heated oil bath at 90 °C and the reaction mixture was magnetically stirred for 5 h. ^{1}H NMR spectroscopy studies indicated ≥ 98% HPMA monomer conversion (the integrated vinyl proton signals at 5.0-6.0 ppm were compared with the integrated polymer backbone signals at 3.5-4.0 ppm). THF GPC analysis indicated an M_n of 18 800 g mol^{-1} and an M_w/M_n of 1.37. Other diblock copolymer compositions were targeted at 15% to 30% w/w solids by using the same molar amount of $PSMA_9$ and adjusting the HPMA/$PSMA_9$ molar ratio and the volume of mineral oil accordingly.

Preparation of Oil-in-Water Pickering Emulsions

Water (1.50 ml, 75% v/v) was homogenized at 20 °C with an 0.03–1.0% w/w $PSMA_9$-$PHPMA_{50}$ diblock copolymer dispersion in mineral oil (0.50 mL) for 2 min at 13 500 rpm using an IKA Ultra-Turrax T-18 homogenizer equipped with a 10 mm dispersing tool. After appropriate dilution, the resulting oil droplets were imaged by optical and fluorescence microscopy and the volume-average droplet diameter was determined by laser diffraction.

Preparation of Water-in-Oil Pickering Emulsions

Water (0.50 mL, 25% v/v) was homogenized in turn with an 0.03–1.0% w/w $PSMA_9$-$PHPMA_{50}$ diblock copolymer dispersion in mineral oil (1.50 mL) for 2 min at 20 °C using an IKA Ultra-Turrax T-18 homogenizer equipped with a 10 mm dispersing tool operating at 13 500 rpm. After appropriate dilution, the resulting aqueous emulsion droplets were imaged by optical and fluorescence microscopy and the volume-average droplet diameter was determined by laser diffraction.

Preparation of Water-in-Oil-in-Water Pickering Double Emulsions

Water (1.0 mL, 50% v/v) was homogenized in turn with an 1.0% w/w $PSMA_9$-$PHPMA_{50}$ diblock copolymer dispersion in mineral oil (10.0 mL) for 2 min at 20 °C using an IKA Ultra-Turrax T-18 homogenizer equipped with a 10 mm dispersing tool. The shear rate was systematically varied between 3 500 rpm and 24 000 rpm. After appropriate dilution, the resulting w/o/w double emulsions were visualized by optical microscopy and fluorescence microscopy.

^{1}H NMR spectroscopy

^{1}H NMR spectra were recorded in either CD_2Cl_2 or $CDCl_3$ using a 400 MHz Bruker Avance III spectrometer. Typically 64 scans were averaged per spectrum. *In situ* ^{1}H NMR spectra were recorded using the same spectrometer in order to study the kinetics of the synthesis of $PSMA_9$-$PHPMA_{150}$ vesicles at 15% w/w solids in mineral oil and also $PSMA_9$-$PBzMA_{150}$ vesicles at 18% w/w solids in the same solvent. A 0.20 mL aliquot of the reaction mixture was transferred into an NMR tube equipped with a J-Young's tap under an inert nitrogen atmosphere. A capillary tube containing 0.28 M toluene dissolved in d_6-DMSO was flame-sealed and used as an external standard (and also a solvent lock). A reference spectrum was recorded at 20 °C prior to heating the reaction mixture up to 90 °C. Spectra were recorded approximately every 2 min for the first 20 min and approximately every 6 min thereafter. Spectra were acquired in eight transients using a 30° excitation pulse and a delay time of 5 s over a spectral window of 16 kHz with 64 k data points.

Gel Permeation Chromatography (GPC)

Molecular weight distributions (MWDs) were assessed by GPC using THF eluent. The THF GPC system was equipped with two 5 µm (30 cm) Mixed C columns and a WellChrom K-2301 refractive index detector operating at 950 ± 30 nm. The THF mobile phase contained 2.0% v/v triethylamine and 0.05% w/v butylhydroxytoluene (BHT) and the flow rate was fixed at 1.0 mL min^{-1}. A series of eleven near-monodisperse poly(methyl methacrylate) standards (M_p values ranging from 800 to 988 000 g mol^{-1}) were used for column calibration.

Dynamic Light Scattering (DLS)

DLS studies were performed using a Zetasizer Nano ZS instrument (Malvern Instruments, UK) at a fixed scattering angle of 173°. Copolymer dispersions were diluted in *n*-dodecane (0.10% w/w) prior to light scattering studies at 25 °C. The intensity-average diameter and polydispersity of the diblock copolymer nanoparticles were calculated by cumulants analysis of the experimental correlation function using Dispersion Technology Software version 6.20. Data were averaged over ten runs each of thirty seconds duration. It is emphasized that DLS assumes a spherical morphology and reports intensity-average diameters. Thus, the DLS diameter determined for highly anisotropic particles such as worms is neither equal to the worm length nor the worm width. Despite this limitation, DLS can be used to monitor a thermally-induced worm-to-sphere transition.[23]

Transmission Electron Microscopy (TEM)

TEM studies were conducted using a FEI Tecnai G2 spirit instrument operating at 80 kV and equipped with a Gatan 1k CCD camera. Diluted diblock copolymer dispersions (0.10%

w/w) were placed on carbon-coated copper grids and exposed to ruthenium(VIII) oxide vapor for 7 min at 20 °C prior to analysis.[59] This heavy metal compound acted as a positive stain for the core-forming block to improve contrast. The ruthenium(VIII) oxide was prepared as follows: ruthenium(IV) oxide (0.30 g) was added to water (50 g) to form a black slurry; addition of sodium periodate (2.0 g) with continuous stirring produced a yellow solution of ruthenium(VIII) oxide within 1 min. In order to study the thermally-induced worm-to-vesicle transition, a sample vial containing 1.0 g of a 25% w/w $PSMA_9$–$PHPMA_{70}$ dispersion in mineral oil was placed in a pre-heated oil bath at 150 °C, allowed to equilibrate for 1 h, diluted with *n*-dodecane (preheated to the same temperature), and then a single droplet of this hot dispersion was transferred onto a TEM grid and allowed to evaporate.

Small-angle X-ray scattering (SAXS)

SAXS patterns were collected at a synchrotron source (Diamond Light Source, station I22, Didcot, UK) using monochromatic X-ray radiation (wavelength λ = 0.100 nm, with q ranging from 0.017 to 2.1 nm^{-1}, where $q = 4\pi.\sin\vartheta/\lambda$ is the length of the scattering vector and ϑ is one-half of the scattering angle) and a 2D Pilatus 2M pixel detector (Dectris, Switzerland). A glass capillary of 2.0 mm diameter was used as a sample holder. Scattering data were reduced using standard routines from the beamline and were further analyzed using Irena SAS macros for Igor Pro.[60]

Oscillatory Rheology

An Anton Paar MCR 502 rheometer (equipped with TruGap functionality for online monitoring of the geometry gap), a variable-temperature Peltier plate, Peltier hood and a 50 mm 2° stainless cone was used for the rheology experiments. The storage (G') and loss (G'') moduli were determined as a function of temperature at a heating rate of 2 °C min^{-1}, a fixed strain amplitude of 1.0%, and an angular frequency of 10 rad s^{-1}. The sample gap was 207 µm.

Optical Microscopy (OM)

Optical microscopy images were recorded using a Cole-Palmer compound optical microscope equipped with an LCD tablet display and a Moticam BTW digital camera.

Fluorescence Microscopy

Fluorescence microscopy images of the w/o precursor emulsion and various w/o/w double Pickering emulsions were recorded using a Zeiss Axio Scope A1 microscope equipped with an AxioCam 1Cm1 monochrome camera. Nile Red dye was dissolved in the mineral oil prior to high-shear homogenization and the resulting oil droplets were imaged using Zeiss filter set 43 HE (excitation 550/25 nm and emission 605/70 nm). Images were captured and processed using ZEN lite 2012 software.

Laser Diffraction

Each o/w and w/o/w emulsion was sized by laser diffraction using a Malvern Mastersizer 3000 instrument equipped with a hydro EV wet sample dispersion unit, a red HeNe laser operating at 633 nm and a LED blue light source operating at 470 nm. The stirring rate was adjusted to 1500 rpm in order to avoid creaming of the emulsion droplets during analysis. After each measurement, the cell was rinsed once with ethanol and three times with deionized water and the laser was aligned centrally to the detector prior to data acquisition.

Results and Discussion

Synthesis of $PSMA_9$ macro-CTA

The RAFT solution polymerization of SMA was conducted in toluene at 70 °C using CPDB as a RAFT CTA to produce the desired PSMA stabilizer precursor (see **Scheme 1**). A preliminary kinetic study when targeting a $PSMA_5$ precursor had indicated first-order kinetics after an initial induction period of approximately 1 h and the expected linear evolution in molecular weight with conversion (see **Figure S1**). In order to avoid the possible loss of RAFT chain-ends under monomer-starved conditions, the scaled-up SMA polymerization was quenched after 4 h by exposure to air, which resulted in an SMA conversion of 77%. This protocol produced approximately 26 g of PSMA homopolymer with a mean degree of polymerization (DP) of 9 and a relatively narrow molecular weight distribution (M_w/M_n = 1.12), indicating that good RAFT control was achieved.

Kinetic study of the RAFT dispersion polymerization of HPMA in mineral oil

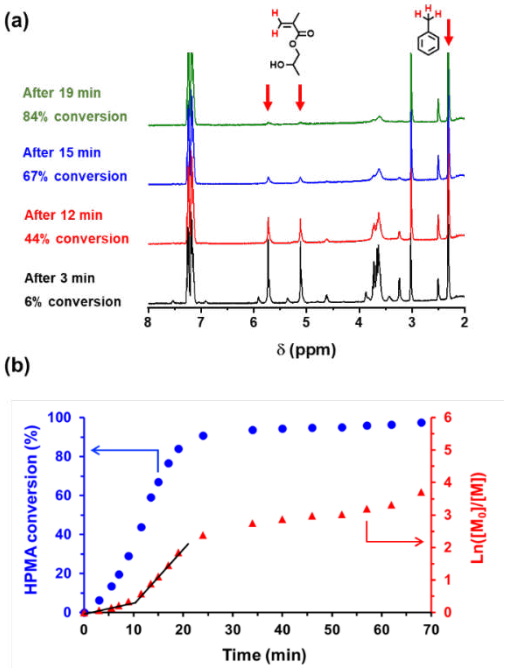

Figure 1. (a) Selected partial ^{1}H NMR spectra recorded during the RAFT dispersion polymerization of HPMA targeting a 15% w/w dispersion of $PSMA_9$-$PHPMA_{150}$ vesicles in mineral oil at 90 °C: after 3 min (black data), 12 min (red data), 15 min (blue data) and 19 min (green data) using toluene in d_6-DMSO as an external standard. **(b)** Conversion *vs.* time curve (blue circles) and corresponding semi-logarithmic plot (red triangles) for the same PISA synthesis.

In situ ^{1}H NMR spectroscopy experiments were performed to examine the kinetics of the RAFT dispersion polymerization of HPMA at 90 °C when targeting PSMA$_9$-PHPMA$_{150}$ vesicles at 15% w/w solids. HPMA conversions were determined by comparing the integrated monomer vinyl proton signals at 5.0-6.0 ppm to the three methyl protons assigned to the toluene external standard at 2.3 ppm (see **Figure 1a**). The HPMA polymerization proceeded relatively slowly for the first 10 min prior to an approximate six-fold rate enhancement. This time point corresponded to 29% HPMA conversion or a PHPMA DP of 44 and is attributed to the onset of micellar nucleation as the growing PHPMA chains become insoluble in the HPMA/mineral oil reaction mixture.[28,32] Thereafter, first-order kinetics were observed up to 84% HPMA conversion, followed by a slower rate of polymerization under monomer-starved conditions (see **Figure 1b**). More than 98% HPMA conversion was achieved within 70 min at 90 °C.

This indicates a significantly faster polymerization than most previously studied PISA formulations in non-polar media, which is attributed to the polar nature of HPMA.[24] In order to confirm this hypothesis, we decided to compare the kinetics of this RAFT dispersion polymerization with that for a non-polar monomer, benzyl methacrylate (BzMA), while targeting PSMA$_9$-PBzMA$_{150}$ vesicles in mineral oil under precisely the same reaction conditions (i.e. using identical monomer and PSMA$_9$ concentrations). For PSMA$_9$-PHPMA$_{150}$ vesicles, an HPMA conversion of 94% was achieved within 40 min whereas only 37% BzMA conversion was achieved for PSMA$_9$-PBzMA$_{150}$ vesicles on the same timescale (see **Figure 2**).

Moreover, the corresponding semilogarithmic plots suggested a pseudo-first order rate constant for the HPMA polymerization that was twelve-fold greater than that for the BzMA polymerization (see **Figure S2**). THF GPC analysis of the final PSMA$_9$-PHPMA$_{150}$ (98% conversion after 70 min; M_n = 19,500 g mol^{-1}, M_w/M_n = 1.24) and PSMA$_9$-PBzMA$_{150}$ diblock copolymers (97% conversion after 150 min; M_n = 17,300 g mol^{-1}, M_w/M_n = 1.11) indicated good RAFT control over these polymerizations in both cases. Thus it appears that the RAFT dispersion polymerization of HPMA offers an advantage over the equivalent synthesis using BzMA.

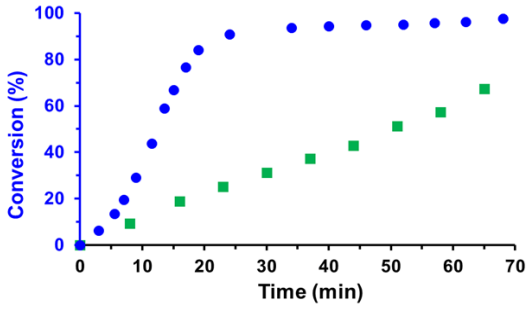

Figure 2. Conversion *vs.* time curves obtained for the RAFT dispersion polymerization of either HPMA (blue circles) or BzMA (green squares) at 90 °C in mineral oil targeting either PSMA$_9$-PHPMA$_{150}$ vesicles at 15% w/w solids or PSMA$_9$-PBzMA$_{150}$ at 18% w/w solids, respectively. Conditions: [HPMA]$_0$ = [BzMA]$_0$ = 0.78 M; [PSMA$_9$] = 17 g dm^{-3}; [PSMA$_9$]/[T21s] molar ratio = 5.0.

Synthesis of PSMA$_9$-PHPMA$_x$ diblock copolymer nanoparticles

A series of PSMA$_9$-PHPMA$_x$ diblock copolymer nano-objects were then targeted *via* RAFT dispersion polymerization of HPMA in mineral oil at 90 °C. The PSMA$_9$ precursor was utilized to polymerize HPMA and PHPMA DPs from 30 to 150 were targeted while varying the overall solids content between 15% and 30% w/w. In each case, more than 98% HPMA monomer conversion was achieved within 5 h as judged by ^{1}H NMR spectroscopy. GPC analysis indicated that relatively good RAFT control was achieved in all cases ($M_w/M_n \leq 1.37$, see **Figure 3**). Targeting higher PHPMA DPs resulted in a systematic shift in the GPC curves towards higher molecular weight (see **Figure 3a**), while minimal PSMA$_9$ precursor contamination indicated high blocking efficiencies. Moreover, a linear evolution of M_n with target PHPMA DP is observed in **Figure 3b** for a series of PSMA$_9$-PHPMA$_x$ nano-objects prepared at 15% w/w solids, although a gradual increase in M_w/M_n is discernible as higher PHPMA DPs are targeted.

Recently, we reported the chain extension of PSMA$_{13}$ and PSMA$_{18}$ stabilizer blocks using glycidyl methacrylate in mineral oil, but only kinetically-trapped spherical nanoparticles could be obtained.[29] In contrast, using the shorter PSMA$_9$ stabilizer block for the RAFT dispersion polymerization of HPMA provides convenient access to worms and vesicles, as well as spheres. Accordingly, a pseudo-phase diagram was constructed to

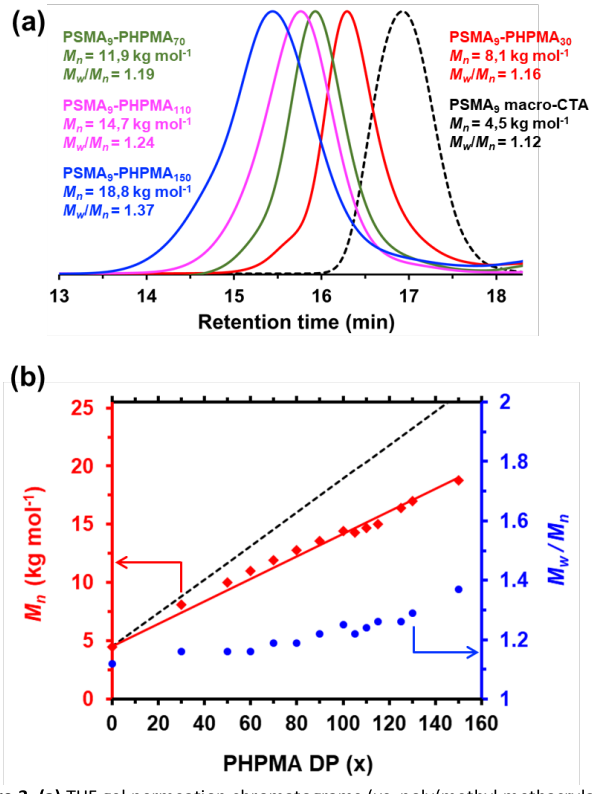

Figure 3. (a) THF gel permeation chromatograms (*vs.* poly(methyl methacrylate) standards) obtained for the precursor PSMA$_9$ macro-CTA (black dashed curve) and four PSMA$_9$-PHPMA$_x$ diblock copolymers prepared *via* RAFT dispersion polymerization of HPMA in mineral oil at 90 °C targeting 15% w/w solids. **(b)** Plots of M_n (red squares) and M_w/M_n (blue circles) *vs.* PHPMA DP for a series of PSMA$_9$-PHPMA$_x$ diblock copolymer nano-objects. The black dashed line indicates the theoretical M_n *vs.* PHPMA DP relationship for this series, with the difference being attributed to the GPC calibration error incurred by using poly(methyl methacrylate) standards.

facilitate the reproducible synthesis of such nano-objects (see **Table S1-S4**), with copolymer morphology assignments being made on the basis of TEM studies (see **Figure 4**).[12,22,28,37] Well-defined spherical nanoparticles could be obtained at all copolymer concentrations examined, with DLS studies indicating narrow size distributions (polydispersity index, PDI ≤ 0.20) and a systematic increase in the intensity-average diameter when targeting higher PHPMA DPs, as expected. [28,29] However, a pure worm phase could only be obtained at relatively high copolymer concentrations (either 25% w/w or 30% w/w solids). Derry *et al.* reported similar observations for poly(lauryl methacrylate)-poly(benzyl methacrylate) diblock copolymer nano-objects prepared in mineral oil.[12] The rather broad mixed phase observed in **Figure 4e** is similar to that recently reported by Rymaruk et al.[31] for polydimethylsiloxane-poly(2-(dimethylamino)ethyl methacrylate) nano-objects in silicone oil. This suggests that sphere-sphere fusion is not particularly efficient for such PISA formulations. Nevertheless, pure vesicles could be accessed by targeting PHPMA DPs of at least 115 at copolymer concentrations ranging from 15% w/w to 25% w/w. Interestingly, a mixed phase comprising vesicles and lamellae was observed when increasing the copolymer concentration up to 30% w/w (see **Figure 4d**).

To confirm the copolymer morphologies assigned by TEM analysis, SAXS patterns were recorded for 1.0% w/w dispersions of four $PSMA_9$–$PHPMA_x$ diblock copolymers originally prepared at 25% w/w (see **Figure 5**).

For $PSMA_9$–$PHPMA_{50}$, an approximate zero gradient was observed at low q as expected for spherical nanoparticles, and the local minimum in the scattering pattern at q ~ 0.5 nm^{-1} indicates a mean core radius of approximately 9 nm.[61] Fitting this SAXS pattern to a well-known spherical micelle model[62] indicated an overall sphere diameter (D_{sphere}) of 21.1 ± 1.9 nm and a mean aggregation number (N_{agg}, or number of copolymer chains per nanoparticle) of 200 (see **Table 1**). This volume-average D_{sphere} value is consistent with the intensity-average diameter of 31 nm reported by DLS for these $PSMA_9$-$PHPMA_{50}$ spheres. The SAXS pattern recorded for $PSMA_9$–$PHPMA_{70}$ exhibits a gradient of approximately -1 in the low q region, which is consistent with the worm morphology indicated by TEM analysis. In this case, the local minimum observed at q ~ 0.4 nm^{-1} represents the mean worm core radius. Fitting this SAXS pattern to a worm-like micelle model[62] indicates an overall worm thickness (T_{worm}) of 22.5 ± 2.4 nm, a mean worm length (L_{worm}) of ~252 nm and an N_{agg} of 3800. Comparing this aggregation number with that determined for the $PSMA_9$-$PHPMA_{50}$ spheres suggests that, on average, approximately 19 spheres undergo stochastic 1D fusion to form each worm. SAXS

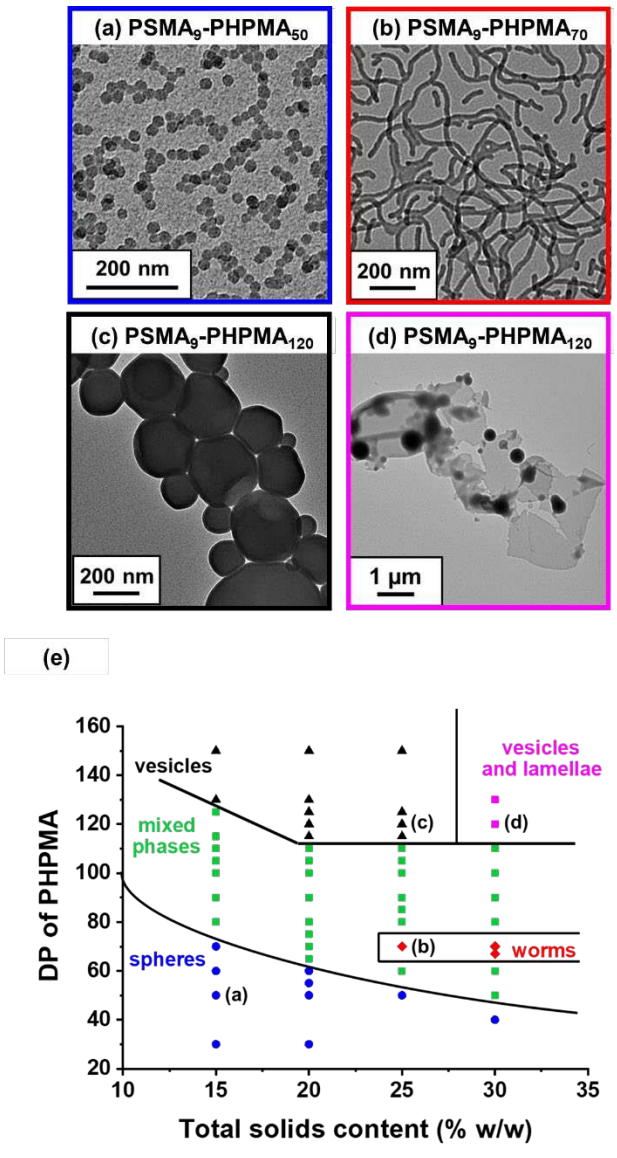

Figure 4. Copolymer morphologies were assigned based on TEM studies. Representative TEM images obtained for **(a)** $PSMA_9$-$PHPMA_{50}$ spheres, **(b)** $PSMA_9$-$PHPMA_{70}$ worms, **(c)** $PSMA_9$-$PHPMA_{120}$ vesicles and **(d)** a mixed phase comprising $PSMA_9$-$PHPMA_{120}$ lamellae and vesicles are shown for reference. **(e)** Pseudo-phase diagram constructed for $PSMA_9$–$PHPMA_x$ diblock copolymer nano-objects prepared by RAFT dispersion polymerization of HPMA in mineral oil using a $PSMA_9$ precursor and T21s initiator at 90 °C ([$PSMA_9$]/[T21s] molar ratio = 5.0). [Black triangles (▲), red diamonds (◆) and blue circles (●) represent pure vesicles, worms and spheres, respectively. Green squares (■) correspond to either sphere/worm or worm/vesicle mixed phases, whereas purple squares (■) represent a vesicle/lamellae mixed phase].

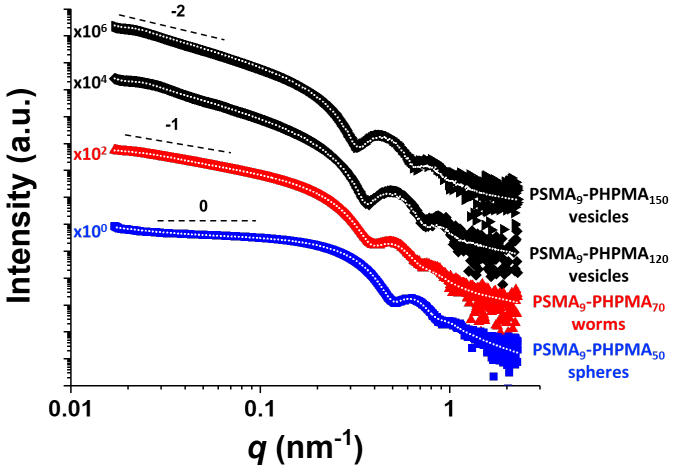

Figure 5. Small-angle X-ray scattering patterns recorded for 1.0% w/w dispersions of $PSMA_9$-$PHPMA_x$ diblock copolymer spheres, worms and vesicles in mineral oil. Dotted lines indicate the data fits obtained using the relevant scattering model. In each case, these diblock copolymer nano-objects were initially synthesized at 25% w/w solids.

Table 1. Summary of nano-object dimensions obtained from fitting small-angle X-ray scattering patterns using either a spherical micelle,[62] worm-like micelle[62] or vesicle model.[63] D_{sphere} is the overall sphere diameter such that $D_{sphere} = 2R_s + 4R_g$, where R_s is the mean core radius and R_g is the radius of gyration of the stabilizer chains. T_{worm} is the overall worm thickness ($T_{worm} = 2R_{wc} + 4R_g$, where R_{wc} is the mean worm core radius) and L_{worm} is the mean worm contour length. $D_{vesicle}$ is the overall vesicle diameter ($D_{vesicle} = 2R_m + T_{membrane} + 4R_g$, where R_m is the distance from the centre of the vesicle to the centre of the vesicle membrane, and $T_{membrane}$ is the vesicle membrane thickness). N_{agg} is the mean aggregation number (i.e. the mean number of copolymer chains per nano-object).

Block copolymer	Nanoparticle Morphology	D_{sphere}	T_{worm}	L_{worm}	$D_{vesicle}$	$T_{membrane}$	N_{agg}
$PSMA_9$-$PHPMA_{50}$	Spheres	21.1 ± 1.9 nm	-	-	-	-	200
$PSMA_9$-$PHPMA_{70}$	Worms	-	22.5 ± 2.4 nm	252 nm	-	-	3800
$PSMA_9$-$PHPMA_{120}$	Vesicles	-	-	-	348 ± 54 nm	16.0 ± 1.6 nm	177,400
$PSMA_9$-$PHPMA_{150}$	Vesicles	-	-	-	366 ± 58 nm	18.1 ± 1.9 nm	177,500

patterns recorded for $PSMA_9$–$PHPMA_{120}$ and $PSMA_9$–$PHPMA_{150}$ both exhibit low q gradients of approximately -2, which is consistent with a vesicular morphology.[28,37] In this case, the subtle feature observed at low q (q ~ 0.02 nm^{-1}) indicates the overall vesicle radius while the well-defined local minimum at high q (q ~ 0.2-0.3 nm^{-1}) provides information regarding the vesicle membrane thickness. Fitting these patterns to a well-known vesicle model[63] indicated that $PSMA_9$–$PHPMA_{120}$ and $PSMA_9$–$PHPMA_{150}$ exhibit comparable overall vesicle diameters ($D_{vesicle}$ = 348 ± 54 nm and 366 ± 58 nm, respectively), but increasing the PHPMA DP from 120 to 150 led to a thicker vesicle membrane ($T_{membrane}$ = 16.0 ± 1.6 nm *vs*. 18.1 ± 1.9 nm, respectively). These data are consistent with the vesicle growth mechanism proposed by Warren *et al.*[64] and later validated by Derry *et al.*[28] for PISA syntheses. Mean N_{agg} values for $PSMA_9$–$PHPMA_{120}$ and $PSMA_9$–$PHPMA_{150}$ vesicles were calculated to be 177,400 and 177,500, respectively. These N_{agg} values are remarkably similar, which suggests that little or no net copolymer chain exchange occurs during the latter stages of the PISA synthesis of $PSMA_9$-$PHPMA_{150}$ vesicles (i.e. from 80% to 100% HPMA conversion). Comparing these N_{agg} values to that obtained for the worms suggest that each vesicle comprises around 47 worms.

Rheological studies of a $PSMA_9$-$PHPMA_{70}$ worm gel

The $PSMA_9$-$PHPMA_{70}$ worms prepared at 25% w/w in mineral oil form a free-standing gel owing to multiple inter-worm contacts.[45] This worm gel was characterized by variable-temperature oscillatory rheology, as described previously for other worm gel systems.[23,35,40] Degelation occurred on heating above approximately 100 °C, with this critical temperature corresponding to the cross-over point for the bulk modulus G' and storage modulus G'' curves (see **Figure 6a**). Similar thermoresponsive behavior has been reported for poly(lauryl methacrylate)-poly(benzyl methacrylate) nano-objects in *n*-dodecane and explained in terms of a *worm-to-sphere* transition owing to surface plasticization of the worm cores by ingress of hot solvent.[23] However, in the present case TEM studies suggest that a partial *worm-to-vesicle* transition occurs on heating. The initial pure worms – diluted at 20 °C for TEM analysis (see **Figure 6b**) – were transformed into a mixed phase comprising large vesicles and some remaining worms on heating up to 150 °C (see **Figure 6c**). These observations are consistent with DLS studies: the sphere-equivalent intensity-average diameter determined at 20 °C for the initial dilute dispersion of pure worms (156 nm, PDI = 0.54) increased significantly after heating up to 150 °C (231 nm, PDI = 0.63). On cooling, regelation occurred at a critical gelation temperature (CGT) of approximately 100 °C, which suggests thermoreversible behavior. However, the initial G' value of ~ 6700 Pa was reduced by more than an order of magnitude to ~ 420 Pa after this single thermal cycle. Moreover, TEM analysis

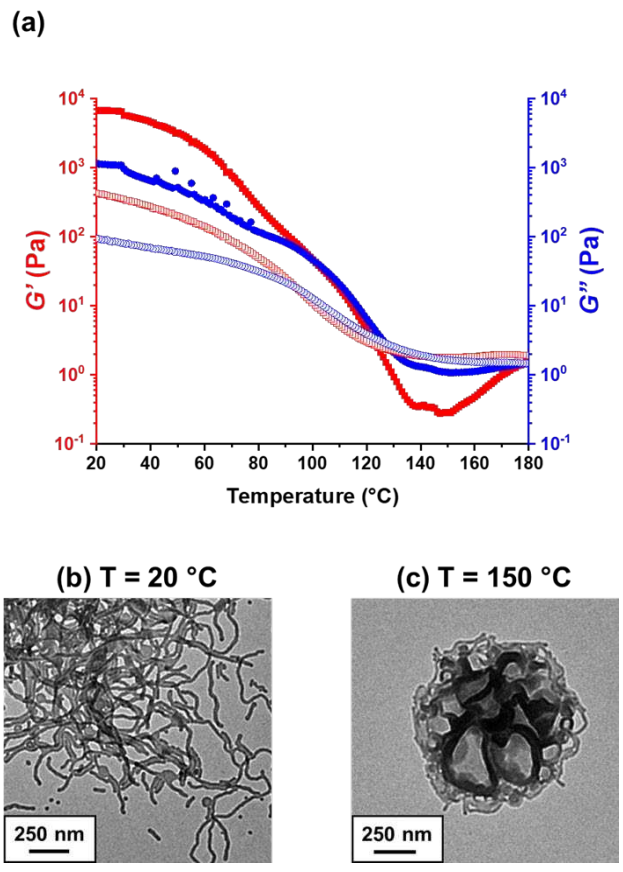

Figure 6. (a) Temperature dependence for the storage moduli (G', red squares) and loss moduli (G'', blue circles) observed for a $PSMA_9$–$PHPMA_{70}$ worm gel prepared at 25% w/w solids in mineral oil on heating from 20 to 180 °C (filled symbols) and cooling from 180 to 20 °C (hollow symbols) at a rate of 2.0 °C min^{-1}. Data were recorded at 1.0% strain amplitude using an angular frequency of 10 rad s^{-1}. Representative TEM images obtained for this $PSMA_9$–$PHPMA_{70}$ dispersion after dilution **(b)** at 20 °C (pure worms) and **(c)** 150 °C (mixed phase comprising vesicles and worms). This partial morphological transition accounts for the degelation that is observed above 100 °C.

of the diluted copolymer dispersion revealed a mixed morphology of worms and vesicles at 20 °C, thus indicating that the original pure worm morphology had not been restored on cooling (see **Figure S3**).

Unlike previous morphological transformations of diblock copolymer nano-objects in non-polar media,[23,27,65,66] this partial worm-to-vesicle transition on heating cannot be explained by surface plasticization of the PHPMA worm cores by hot solvent. This can only result in an increase in the volume of the solvophilic block relative to the solvophobic block, resulting in a reduction in the critical packing parameter (*P*) and thus favoring the formation of spheres. Instead, an *increase* in *P* is required to generate vesicles from the initial worms, which means that the relative volume of the solvophobic PHPMA block must increase relative to that of the solvophilic PSMA block. In principle, this could occur *via uniform solvation* of the core-forming PHPMA block. However, this seems unlikely given that even hot *n*-dodecane is likely to remain a very poor solvent for the hydroxyl-functional PHPMA chains. An alternative explanation could be that the poly(lauryl methacrylate) block becomes slightly less solvated at elevated temperature and hence occupies a smaller volume relative to that at 20 °C. Clearly, further studies are warranted to provide a satisfactory physical explanation for this unexpected morphological transition, which serves to demonstrate that there is still much to learn about such thermoresponsive PISA formulations.

$PSMA_9$-$PHPMA_{50}$ diblock copolymer spheres as putative Pickering emulsifiers

$PSMA_9$-$PHPMA_{50}$ diblock copolymer spheres prepared at 15% w/w copolymer concentration in mineral oil were evaluated as a putative Pickering emulsifier. In some respects such nanoparticles are quite similar to the $PSMA_{14}$-$PNMEP_{49}$ diblock copolymer spheres prepared in *n*-dodecane by Cunningham *et al*.[24] In both cases the PSMA stabilizer block is relatively short and the core-forming block is relatively polar, with PNMEP being water-soluble[67] and PHPMA being only weakly hydrophobic.[68]

Cunningham *et al*.[24] reported that *hydrophobic* $PSMA_{14}$-$PNMEP_{49}$ spherical nanoparticles unexpectedly formed *oil-in-water* Pickering emulsions when subjected to high-shear homogenization with water. This observation was attributed to *in situ* inversion of the diblock copolymer nanoparticles to produce *hydrophilic* $PNMEP_{49}$-$PSMA_{14}$ spheres.[24] In contrast, when emulsification was conducted under low shear (*via* hand-shaking), the anticipated *water-in-oil* Pickering emulsion was formed. Furthermore, using relatively low water volume fractions (e.g. ≤ 0.25) also enabled the preparation of *water-in-oil* emulsions. There are two key differences between the current study and that reported by Cunningham *et al*.[24] Firstly, the current diblock copolymer spheres are prepared in mineral oil rather than *n*-dodecane. Perhaps more importantly, the nanoparticle cores are composed of PHPMA chains, which – unlike PNMEP – do not become hydrophilic under any conditions. Hence inversion of the diblock copolymer chains to form $PHPMA_{50}$-$PSMA_9$ nanoparticles is not expected to occur in the present study, which should lead to differing Pickering emulsifier behavior.

First, the effect of varying the water volume fraction on Pickering emulsion formation was studied. A series of emulsions was prepared *via* high-shear homogenization at 13 500 rpm for 2 min using a fixed 1.0% w/w dispersion of $PSMA_9$-$PHPMA_{50}$ spheres in mineral oil and water volume fractions ranging from 0.135 to 0.875 (see **Scheme 2**). **Figure S4** shows digital photographs of the physical appearance of the resulting emulsions, which were visualized using optical and fluorescent microscopy (see **Figure 7**). The digital photograph of the emulsion prepared at a water volume fraction of 0.25 indicates the formation of a water-in-oil emulsion because the denser water droplets sediment to form the lower phase, which has a smaller volume. Optical microscopy images recorded for this emulsion indicated a mean droplet diameter of around 25 µm. To aid identification of the emulsion type, Nile Red dye was dissolved in the mineral oil prior to homogenization to enable fluorescence microscopy studies. As shown in **Figure 7d**, this fluorescent label is mainly located in the continuous phase, confirming that a water-in-oil emulsion is obtained in this case. In contrast, an emulsion prepared at a water volume fraction of 0.50 comprised relatively large fluorescently-labelled droplets, suggesting formation of an oil-in-water emulsion under such conditions, see **Figure 7e**. However, closer inspection revealed that spherical water droplets were present within these coarse oil droplets, indicating that a water-in-oil-in-water (w/o/w) double emulsion had been formed. Literature examples of the

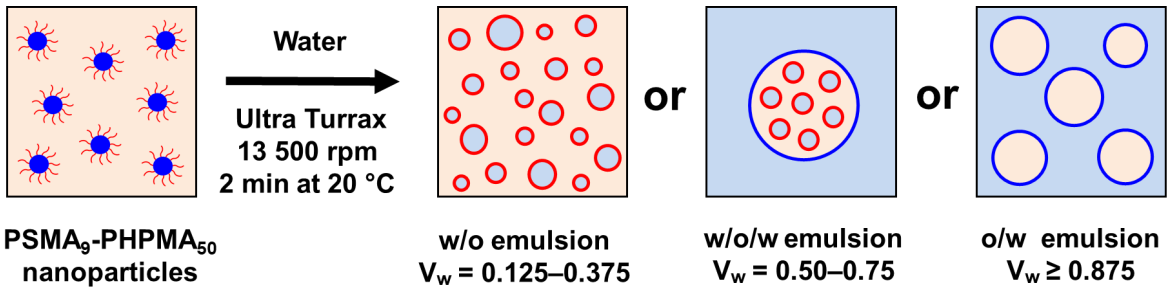

Scheme 2. Schematic representation of the three types of Pickering emulsions that can be formed when using $PSMA_9$-$PHPMA_{50}$ spherical nanoparticles synthesized directly in mineral oil *via* RAFT dispersion polymerization of HPMA. Systematic adjustment of the volume fraction of the aqueous phase enables the preparation of water-in-oil (water volume fraction = 0.125 to 0.375), water-in-oil-in-water (water volume fraction = 0.50 to 0.75) or oil-in-water (water volume fraction ≥ 0.875) Pickering emulsions.

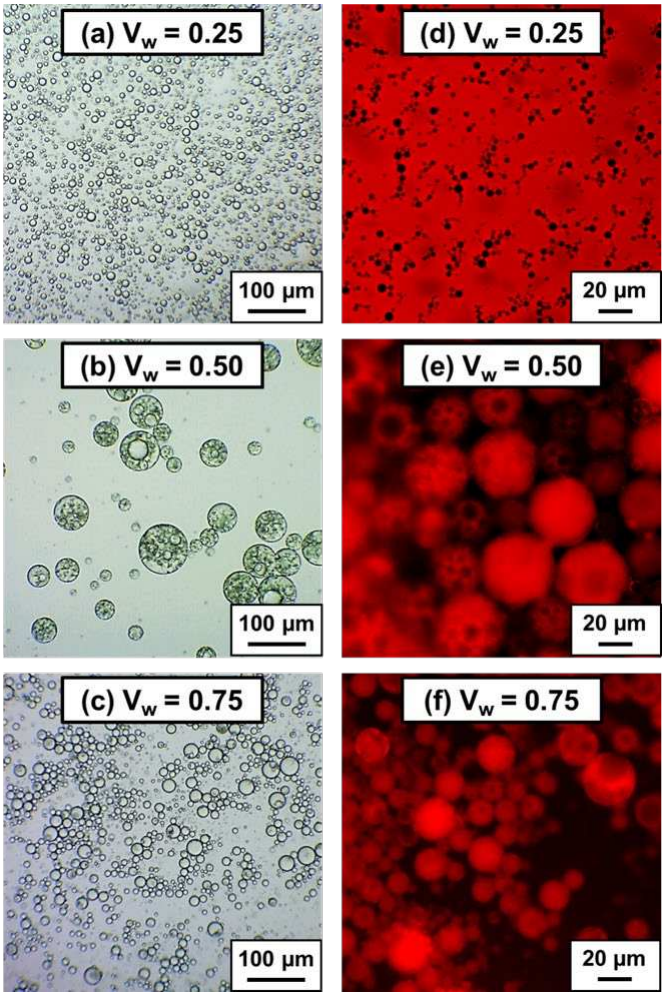

Figure 7. (a-c) Optical microscopy images and **(d-f)** fluorescence microscopy images recorded for Pickering emulsions prepared by high-shear homogenization of 1.00% w/w $PSMA_9$-$PHPMA_{50}$ spheres in mineral oil using water volume fractions (V_w) of 0.25, 0.50 or 0.75. In each case, the oil phase has been labelled with a water-insoluble dye (Nile Red). For a water volume fraction of 0.25, black aqueous droplets are observed within a continuous phase comprising the mineral oil and this red dye. However, when emulsions are prepared at a water volume fraction of 0.50, red oil droplets are observed within a dark aqueous continuous phase. Moreover, water droplets are visible within these dyed oil droplets, indicating the formation of w/o/w double emulsions. Similar w/o/w double emulsions are produced at a water volume fraction of 0.75, albeit containing fewer encapsulated aqueous droplets.

one-step formation of such complex emulsions using a *single* emulsifier are known but are relatively rare.[69–74] Employing a water volume fraction of 0.75 produced a double emulsion, albeit with significantly fewer encapsulated aqueous droplets, as shown in **Figure 7f**. Increasing the water volume fraction to 0.875 appeared to produce a simple oil-in-water emulsion, as judged by optical microscopy. However, fluorescence microscopy studies indicated the presence of encapsulated aqueous droplets within at least some of the oil droplets, indicating that a double emulsion was in fact obtained (see **Figure S5**).

According to the literature, high-shear homogenization of diblock copolymer nano-objects can cause *in situ* dissociation in some cases, which leads to the formation of emulsion droplets stabilized by *individual* diblock copolymer chains acting as a polymeric surfactant. [52,53,55,75] Moreover, such instances typically involve PHPMA-core nanoparticles, albeit those prepared *via* aqueous PISA formulations rather than the present non-aqueous formulation.[52,53,55] Fortunately, whether such nano-object dissociation actually occurs in practice can be assessed by determining the variation in mean droplet diameter with copolymer concentration.[53,55,70,76] To examine whether genuine Pickering emulsions are formed in the present study, the copolymer concentration was systematically varied between 0.03% and 1.00% w/w in mineral oil. These dispersions were homogenized using a water volume fraction of 0.75, 0.50 or 0.25 at a constant shear rate of 13 500 rpm to produce a series of either w/o single emulsions or w/o/w double emulsions. **Figure S6** shows a representative digital photograph recorded for the resulting emulsions. Droplet size distributions for the w/o/w emulsions were analyzed using laser diffraction, as shown in **Figure 8**. Systematically increasing the copolymer concentration led to gradual reduction in the mean droplet diameter until a limiting value of approximately 25 µm was attained at 1.00% w/w [$PSMA_9$-$PHPMA_{50}$]. Similar results were obtained for water-in-oil emulsions prepared at a water volume fraction of 0.25 (see **Figure S7**). These observations are consistent with the corresponding optical microscopy images (see inset) and indicate that the nanoparticles remain intact after high-shear homogenization, leading to the formation of genuine Pickering emulsions.

To examine the effect of copolymer concentration on the formation of Pickering double emulsions, a series of emulsions were prepared at a constant water volume fraction of 0.50 using a stirring rate of 13 500 rpm for 2 min. The resulting emulsion droplets were imaged using fluorescence microscopy, see **Figure 9**. Preparing the emulsions at 0.03% w/w copolymer concentration produced relatively large w/o single emulsions of approximately 150 µm diameter, as confirmed by the presence

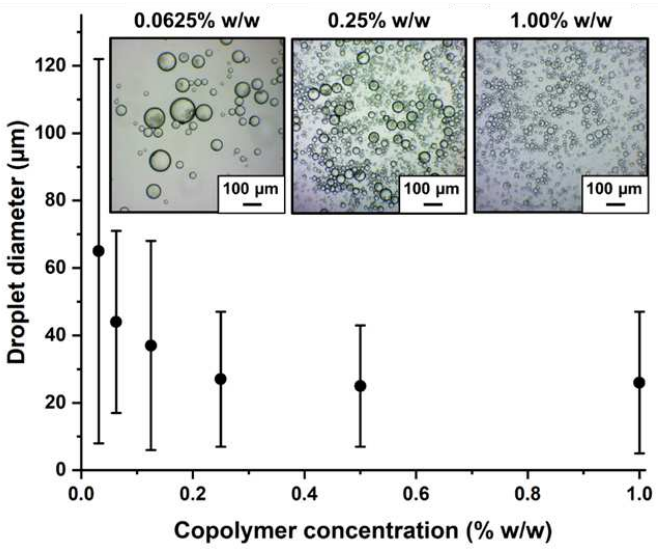

Figure 8. Variation in volume-average droplet diameter (determined by laser diffraction studies) with copolymer concentration obtained for water-in-oil-in-water (w/o/w) Pickering double emulsions produced *via* high-shear homogenization (13 500 rpm for 2 min at 20 °C) of $PSMA_9$-$PHPMA_{50}$ diblock copolymer spheres in mineral oil at a constant water volume fraction of 0.75. Inset: representative optical microscopy images recorded for such w/o/w emulsions prepared using copolymer concentrations of 0.0625, 0.25 or 1.00% w/w, respectively.

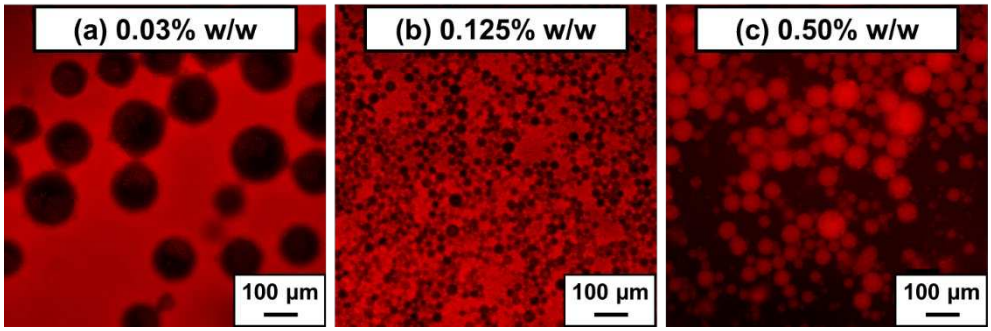

Figure 9. Fluorescence microscopy images recorded for emulsions prepared using $PSMA_9$-$PHPMA_{50}$ spheres at a copolymer concentration of **(a)** 0.03% w/w, **(b)** 0.125% w/w or **(c)** 0.50% w/w. In each case, the water volume fraction was fixed at 0.50 and a constant stirring rate of 13 500 rpm was used for 2 min during high-shear homogenization at 20 °C.

of the Nile Red label in the continuous phase. Increasing the copolymer concentration up to 0.125% w/w led to a systematic reduction in the mean droplet diameter to around 20 µm (see **Figure 9b**), suggesting that the nanoparticles also survive high-shear homogenization when prepared at a water volume fraction of 0.50. However, increasing the copolymer concentration further led to the formation of w/o/w double emulsions, see **Figure 9c**. Thus, either w/o single emulsions or w/o/w double emulsions can be prepared at a constant water volume fraction by simply varying the copolymer concentration.

Finally, the effect of varying the shear rate on emulsion formation was examined. A series of four emulsions were prepared at a constant copolymer concentration of 1.00% w/w and a water volume fraction of 0.50 using shear rates ranging from 3500 rpm to 20 000 rpm. Nile Red was again used to dye the mineral oil prior to emulsification to facilitate fluorescence microscopy studies. For emulsions prepared at relatively low shear (*i.e.*, 3 500 or 7 500 rpm), this dye is located within the continuous phase, confirming the formation of water-in-oil emulsions, see **Figure S8**. As anticipated, w/o/w emulsions are formed at a stirring rate of 15 500 rpm, with dark aqueous domains being clearly visible within the dyed oil droplets. Finally, a stirring rate of 20 000 rpm did not produce significantly smaller oil droplets but there is some evidence for a higher density of encapsulated water domains within the oil droplets.

Conclusions

The PISA synthesis of PSMA-PHPMA diblock copolymer spheres, worms and vesicles was achieved *via* RAFT dispersion polymerization of HPMA at 90 °C in mineral oil. *In situ* ^{1}H NMR spectroscopy was utilized to examine the kinetics of the PISA synthesis of $PSMA_9$-$PHPMA_{150}$ vesicles, for which (≥ 98%) monomer conversion was achieved within 70 min. This is a remarkably short time scale compared to most other PISA formulations conducted in non-polar media and is attributed to the relatively polar nature of the HPMA monomer. Construction of a pseudo-phase diagram for such PSMA-PHPMA diblock copolymer nano-objects enables the reproducible targeting of pure spheres, worms or vesicles, as confirmed by TEM, DLS and SAXS studies. Thus this is the first example of the use of a commercially available polar monomer for PISA syntheses in non-polar media that offers access to the full range of copolymer morphologies. The worms formed thermoresponsive free-standing gels with degelation occurring on heating above 100 °C. Unusually, such degelation is accompanied by a worm-to-vesicle transition, rather than a worm-to-sphere transition. Finally, $PSMA_9$-$PHPMA_{50}$ spheres were evaluated as Pickering emulsifiers. Water-in-oil emulsions were obtained at relatively low water volume fractions (0.125 to 0.375). At higher volume fractions (0.50 to 0.875), a series of water-in-oil-in-water Pickering double emulsions were obtained with progressively fewer encapsulated aqueous droplets. Using either higher shear rates or a higher copolymer concentration during homogenization also favoured the formation of such double emulsions.

Conflicts of interest

There are no conflicts to declare.

Acknowledgements

We thank EPSRC for CDT PhD studentships to support C.G. and S.J.H. (EP/L016281) and The Lubrizol Corporation Ltd. for further financial support of this project and for permission to publish these results. S.P.A. acknowledges an EPSRC *Established Career* Particle Technology Fellowship (EP/R003009) and also the Leverhulme Trust (RPG-2016-330) for post-doctoral support of M.J.D. Dr. S. van Meurs is thanked for her assistance with the *in situ* NMR experiments. The authors thank C. J. Hill and Dr. S. Tzokov at the University of Sheffield Biomedical Science Electron Microscopy suite. We gratefully acknowledge Diamond Light Source for granting synchrotron beamtime (SM14892) and thank the personnel of I22 for their kind assistance.

References

1 S. Krause, *J. Phys. Chem.*, 1964, **68**, 1948–1955.
2 Z. Tuzar and P. Kratochvíl, *Adv. Colloid Interface Sci.*, 1976, **6**, 201–232.
3 Y.-Y. Won, H. T. Davis and F. S. Bates, *Science*, 1999, **283**,

960–963.
4 L. Zhang and A. Eisenberg, *Science*, 1995, **268**, 1728–1731.
5 D. E. Discher and A. Eisenberg, *Science*, 2002, **297**, 967–973.
6 M. Antonietti and S. Förster, *Adv. Mater.*, 2003, **15**, 1323–1333.
7 V. Bütün, S. P. Armes and N. C. Billingham, *Polymer*, 2001, **42**, 5993–6008.
8 J. R. Howse, R. A. L. Jones, G. Battaglia, R. E. Ducker, G. J. Leggett and A. J. Ryan, *Nat. Mater.*, 2009, **8**, 507–511.
9 B. Charleux, G. Delaittre, J. Rieger and F. D'Agosto, *Macromolecules*, 2012, **45**, 6753–6765.
10 M. J. Monteiro and M. F. Cunningham, *Macromolecules*, 2012, **45**, 4939–4957.
11 N. J. Warren and S. P. Armes, *J. Am. Chem. Soc.*, 2014, **136**, 10174–10185.
12 M. J. Derry, L. A. Fielding and S. P. Armes, *Polym. Chem.*, 2015, **6**, 3054–3062.
13 J. Chiefari, Y. K. B. Chong, F. Ercole, J. Krstina, J. Jeffery, T. P. T. Le, R. T. A. Mayadunne, G. F. Meijs, C. L. Moad, G. Moad, E. Rizzardo and S. H. Thang, *Macromolecules*, 1998, **31**, 5559–5562.
14 G. Moad, E. Rizzardo and S. H. Thang, *Aust. J. Chem.*, 2005, **58**, 379–410.
15 G. Moad, E. Rizzardo and S. H. Thang, *Acc. Chem. Res.*, 2008, **41**, 1133–1142.
16 S. L. Canning, G. N. Smith and S. P. Armes, *Macromolecules*, 2016, **49**, 1985–2001.
17 N. J. W. Penfold, J. Yeow, C. Boyer and S. P. Armes, *ACS Macro Lett.*, 2019, **8**, 1029–1054.
18 F. D'Agosto, J. Rieger and M. Lansalot, *Angew. Chemie - Int. Ed.*, , DOI:10.1002/anie.201911758.
19 E. R. Jones, M. Semsarilar, P. Wyman, M. Boerakker and S. P. Armes, *Polym. Chem.*, 2016, **7**, 851–859.
20 N. Zaquen, W. A. A. Azizi, J. Yeow, R. P. Kuchel, T. Junkers, P. B. Zetterlund and C. Boyer, *Polym. Chem.*, 2019, **10**, 2406–2414.
21 J. Yeow and C. Boyer, *Adv. Sci.*, 2017, **4**, 1700137.
22 L. A. Fielding, M. J. Derry, V. Ladmiral, J. Rosselgong, A. M. Rodrigues, L. P. D. Ratcliffe, S. Sugihara and S. P. Armes, *Chem. Sci.*, 2013, **4**, 2081–2087.
23 L. A. Fielding, J. A. Lane, M. J. Derry, O. O. Mykhaylyk and S. P. Armes, *J. Am. Chem. Soc.*, 2014, **136**, 5790–5798.
24 V. J. Cunningham, S. P. Armes and O. M. Musa, *Polym. Chem.*, 2016, **7**, 1882–1891.
25 M. J. Derry, L. A. Fielding and S. P. Armes, *Prog. Polym. Sci.*, 2016, **52**, 1–18.
26 E. J. Cornel, S. Van Meurs, T. Smith, P. S. O. Hora and S. P. Armes, *J. Am. Chem. Soc.*, 2018, **140**, 12980–12988.
27 M. J. Derry, O. O. Mykhaylyk and S. P. Armes, *Angew. Chemie - Int. Ed.*, 2017, **56**, 1746–1750.
28 M. J. Derry, L. A. Fielding, N. J. Warren, C. J. Mable, A. J. Smith, O. O. Mykhaylyk and S. P. Armes, *Chem. Sci.*, 2016, **7**, 5078–5090.
29 P. J. Docherty, M. J. Derry and S. P. Armes, *Polym. Chem.*, 2019, **10**, 603–611.
30 M. J. Derry, T. Smith, P. S. O'Hora and S. P. Armes, *ACS Appl. Mater. Interfaces*, 2019, **11**, 33364–33369.
31 M. J. Rymaruk, S. J. Hunter, C. T. O'Brien, S. L. Brown, C. N. Williams and S. P. Armes, *Macromolecules*, 2019, **52**, 2822–2832.
32 A. Blanazs, J. Madsen, G. Battaglia, A. J. Ryan and S. P. Armes, *J. Am. Chem. Soc.*, 2011, **133**, 16581–16587.
33 A. Blanazs, R. Verber, O. O. Mykhaylyk, A. J. Ryan, J. Z. Heath, C. W. I. Douglas and S. P. Armes, *J. Am. Chem. Soc.*, 2012, **134**, 9741–9748.
34 J. R. Lovett, N. J. Warren, S. P. Armes, M. J. Smallridge and R. B. Cracknell, *Macromolecules*, 2016, **49**, 1016–1025.
35 R. Verber, A. Blanazs and S. P. Armes, *Soft Matter*, 2012, **8**, 9915–9922.
36 N. J. Warren, M. J. Derry, O. O. Mykhaylyk, J. R. Lovett, L. P. D. Ratcliffe, V. Ladmiral, A. Blanazs, L. A. Fielding and S. P. Armes, *Macromolecules*, 2018, **51**, 8357–8371.
37 N. J. Warren, O. O. Mykhaylyk, D. Mahmood, A. J. Ryan and S. P. Armes, *J. Am. Chem. Soc.*, 2014, **136**, 1023–1033.
38 R. Deng, Y. Ning, E. R. Jones, V. J. Cunningham, N. J. W. Penfold and S. P. Armes, *Polym. Chem.*, 2017, **8**, 5374–5380.
39 C. P. Jesson, C. M. Pearce, H. Simon, A. Werner, V. J. Cunningham, J. R. Lovett, M. J. Smallridge, N. J. Warren and S. P. Armes, *Macromolecules*, 2017, **50**, 182–191.
40 L. P. D. Ratcliffe, K. J. Bentley, R. Wehr, N. J. Warren, B. R. Saunders and S. P. Armes, *Polym. Chem.*, 2017, **8**, 5962–5971.
41 N. J. W. Penfold, J. R. Lovett, N. J. Warren, P. Verstraete, J. Smets and S. P. Armes, *Polym. Chem.*, 2016, **7**, 79–88.
42 D. Zehm, L. P. D. Ratcliffe and S. P. Armes, *Macromolecules*, 2013, **46**, 128–139.
43 S. Rimmer, S.-P. Wilshaw, P. Pickavance and E. Ingham, *Biomaterials*, 2009, **30**, 2468–2478.
44 M. Sponchioni, C. T. O'Brien, C. Borchers, E. Wang, M. N. Rivolta, N. J. W. Penfold, I. Canton and S. P. Armes, *Chem. Sci.*, 2020, **11**, 232–240.
45 J. R. Lovett, M. J. Derry, P. Yang, F. L. Hatton, N. J. Warren, P. W. Fowler and S. P. Armes, *Chem. Sci.*, 2018, **9**, 7138–7144.
46 I. Canton, N. J. Warren, A. Chahal, K. Amps, A. Wood, R. Weightman, E. Wang, H. Moore and S. P. Armes, *ACS Cent. Sci.*, 2016, **2**, 65–74.
47 D. E. Mitchell, J. R. Lovett, S. P. Armes and M. I. Gibson, *Angew. Chemie*, 2016, **128**, 2851–2854.
48 K. A. Simon, N. J. Warren, B. Mosadegh, M. R. Mohammady, G. M. Whitesides and S. P. Armes, *Biomacromolecules*, 2015, **16**, 3952–3958.
49 S. U. Pickering, *J. Chem. Soc. Trans.*, 1907, **91**, 2001–2021.
50 W. Ramsden, *Proc. R. Soc. London*, 1903, **72**, 156–164.
51 B. P. Binks, *Curr. Opin. Colloid Interface Sci.*, 2002, **7**, 21–41.
52 K. L. Thompson, P. Chambon, R. Verber and S. P. Armes, *J. Am. Chem. Soc.*, 2012, **134**, 12450–12453.
53 K. L. Thompson, C. J. Mable, A. Cockram, N. J. Warren, V. J. Cunningham, E. R. Jones, R. Verber and S. P. Armes, *Soft Matter*, 2014, **10**, 8615–8626.
54 V. J. Cunningham, A. M. Alswieleh, K. L. Thompson, M. Williams, G. J. Leggett, S. P. Armes and O. M. Musa,

Macromolecules, 2014, **47**, 5613–5623.
55 S. J. Hunter, K. L. Thompson, J. R. Lovett, F. L. Hatton, M. J. Derry, C. Lindsay, P. Taylor and S. P. Armes, *Langmuir*, 2019, **35**, 254–265.
56 K. L. Thompson, J. A. Lane, M. J. Derry and S. P. Armes, *Langmuir*, 2015, **31**, 4373–4376.
57 K. L. Thompson, L. A. Fielding, O. O. Mykhaylyk, J. A. Lane, M. J. Derry and S. P. Armes, *Chem. Sci.*, 2015, **6**, 4207–4214.
58 K. L. Thompson, C. J. Mable, J. A. Lane, M. J. Derry, L. A. Fielding and S. P. Armes, *Langmuir*, 2015, **31**, 4137–4144.
59 J. S. Trent, *Macromolecules*, 1984, **17**, 2930–2931.
60 J. Ilavsky and P. R. Jemian, *J. Appl. Crystallogr.*, 2009, **42**, 347–353.
61 O. Glatter and O. Kratky, *Small-angle X-ray scattering*, Academic Press, London, 1982.
62 J. S. Pedersen, *J. Appl. Crystallogr.*, 2000, **33**, 637–640.
63 J. Bang, S. Jain, Z. Li, T. P. Lodge, J. S. Pedersen, E. Kesselman and Y. Talmon, *Macromolecules*, 2006, **39**, 1199–1208.
64 N. J. Warren, O. O. Mykhaylyk, A. J. Ryan, M. Williams, T. Doussineau, P. Dugourd, R. Antoine, G. Portale and S. P. Armes, *J. Am. Chem. Soc.*, 2015, **137**, 1929–1937.
65 Y. Pei, O. R. Sugita, L. Thurairajah and A. B. Lowe, *RSC Adv.*, 2015, **5**, 17636–17646.
66 Y. Pei, A. B. Lowe and P. J. Roth, *Macromol. Rapid Commun.*, 2017, **38**, 1600528.
67 R. R. Gibson, S. P. Armes, O. M. Musa and A. Fernyhough, *Polym. Chem.*, 2019, **10**, 1312–1323.
68 J. Madsen, S. P. Armes, K. Bertal, S. Macneil and A. L. Lewis, *Biomacromolecules*, 2009, **10**, 1875–1887.
69 P. S. Clegg, J. W. Tavacoli and P. J. Wilde, *Soft Matter*, 2016, **12**, 998–1008.
70 B. P. Binks and C. P. Whitby, *Langmuir*, 2004, **20**, 1130–1137.
71 L. Hong, G. Sun, J. Cai and T. Ngai, *Langmuir*, 2012, **28**, 2332–2336.
72 F. Tu and D. Lee, *Chem. Commun.*, 2014, **50**, 15549–15552.
73 Y. Nonomura, N. Kobayashi and N. Nakagawa, *Langmuir*, 2011, **27**, 4557–4562.
74 S. Kim, K. Kim and S. Q. Choi, *Soft Matter*, 2018, **14**, 1094–1099.
75 C. J. Mable, N. J. Warren, K. L. Thompson, O. O. Mykhaylyk and S. P. Armes, *Chem. Sci.*, 2015, **6**, 6179–6188.
76 R. Aveyard, B. P. Binks and J. H. Clint, *Adv. Colloid Interface Sci.*, 2003, **100**, 503–546.

